Abstract

In this study we consider the boundary-layer flow of an inelastic non-Newtonian fluid over an inclined flat plate. Using two popular generalised Newtonian models we determine base flow profiles and associated linear stability results for a range shear-thinning fluids. In addition to neutral stability curves we also present results concerning the linear growth of the Tollmien-Schlichting waves as they propagate downstream. Furthermore, to gain an insight into the underlying physical mechanisms affecting the destabilisation of the disturbances, an integral energy equation is derived and energy calculations are presented. Results from all three analyses suggest that the effect of shear-thinning will act to stabilise the boundary-layer flow. Consequently, it can be argued that the addition of shear-thinning agents could act as a passive control mechanism for flows of this nature.

Stability of the shear-thinning boundary-layer flow over a flat inclined plate

September 20, 2017

1 Introduction

The study of non-Newtonian boundary-layer flows has received recent interest for numerous reasons. Not only are these flows of particular mathematical intrigue, due to the relative complexity of the boundary-layer equations, they also offer the potential to serve as a passive control mechanism. Indeed, a number of previous studies have shown that the effect of shear-thinning can delay the onset of instability in confined shear flows. For example, Nouar *et al.* [1], Nouar & Frigaard [2], and Alibenyahia *et al.* [3] demonstrate that under certain circumstances, Poiseuille flow, Couette-Poiseuille flow, and Taylor-Couette flow can be stabilised by fluids that exhibit shear-thinning behaviour. In each of the aforementioned studies the authors note the importance of: (i) accounting for the viscosity disturbance when deriving the linear perturbation equations, and (ii) utilising an appropriate viscosity scale in the definition of the Reynolds number. Both of these factors are accounted for within this investigation.

More recent studies have addressed the linear stability characteristics of unconfined non-Newtonian shear flows. The effect of shear-thinning has been shown to delay the onset of convective instability when considering the three dimensional boundary-layer flow due to a rotating disk; see, for example, Griffiths *et al.* [4] and Griffiths *et al.* [5]. However, the results presented in these investigations consider only the 'power-law' formulation of the problem. In the limit of vanishing shear-rate, the power-law model is unable to accurately describe the variation of non-Newtonian viscosity across the boundary-layer, as was first noted by Acrivos *et al.* [6]. Denier & Dabrowski [7] have shown that this failing of the model is intrinsically linked to the slow algebraic decay of the boundary layer solutions. The authors note that a viscous diffusion layer must be introduced in order for the inner algebraically decaying solutions to match with the outer uniform flow. In subsequent investigations Griffiths and co-workers suggest that this unphysical variation of viscosity across the boundary layer may lead to an over prediction of the relative stabilising benefits of shear-thinning flow.

The aim of the present work is to quantify the stabilising (or destabilising) effects of shear-thinning for unbounded shear flows. The numerical framework presented herein allows for a direct comparison between results owing from both the power-law and Carreau non-Newtonian models. The outline of this paper is a follows: In §2 we formulate the problem, solve the boundary-layer equations in a self-similar fashion, and derive the appropriate linear stability equations. We present results regarding neutral stability and linear growth rates in §3. An energy analysis is then presented in §4. All results are discussed and our findings are concluded in §5.

2 Formulation

Consider the flow of an incompressible, shear-thinning, non-Newtonian fluid over an impermeable, semi-infinite, flat plate inclined at an angle $m\pi/(m+1)$, where m is the usual two-dimensional, Falkner-Skan, pressure-gradient parameter. The streamwise coordinate is x^* and the wall normal coordinate is y^* (asterisks denotes dimensional quantities). This flow is depicted schematically in figure 1 and is governed by the continuity and Cauchy momentum equations

$$\boldsymbol{\nabla}^* \boldsymbol{\cdot} \boldsymbol{u}^* = 0, \tag{1a}$$

$$\rho^* \left(\frac{\partial}{\partial t^*} + \boldsymbol{u}^* \boldsymbol{\cdot} \boldsymbol{\nabla}^* \right) \boldsymbol{u}^* = -\boldsymbol{\nabla}^* p^* + \boldsymbol{\nabla}^* \boldsymbol{\cdot} \boldsymbol{\tau}^*. \tag{1b}$$

For flows of this nature the deviatoric stress tensor is defined as

$$\boldsymbol{\tau}^* = \mu(\dot{\gamma}^*)\dot{\boldsymbol{\gamma}}^*,$$

where $\dot{\gamma}^*$ is the second invariant of the strain-rate tensor $\dot{\boldsymbol{\gamma}}^*$. The constitutive viscosity relations considered herein are described by the Ostwald-de Waele power-law model and the modified Carreau model[1]

$$\mu_p^* = k^* |\dot{\gamma}^*|^{n-1}, \quad \mu_c^* = \mu_0^* [1 + (\lambda^* \dot{\gamma}^*)^2]^{(n-1)/2}.$$

In both cases the fluid index n represents the degree of shear-thinning. A Newtonian viscosity relationship is recovered when $n = 1$ and, equivalently, when $\lambda^* = 0$. The consistency coefficient k^*, the zero-shear-rate viscosity μ_0^*, and the characteristic time coefficient λ^*, are all material constants. Throughout the remainder of this analysis it is understood that the subscript p denotes terms associated with the power-law model whilst the subscript c denotes terms associated with the Carreau fluid model.

For the sake of brevity we do not derive the governing boundary-layer equations here. Instead the interested reader is referred to the thorough account provided by Dabrowski [8]. For two-dimensional flows such as this the inviscid

[1] as is commonplace in the literature we assume that the viscosity at zero-shear-rate is much greater than that at infinite-shear-rate ($\mu_0^* \gg \mu_\infty^*$). Here μ_∞^*, denotes the limiting constant viscosity that is recovered at infinitely large shear-rates.

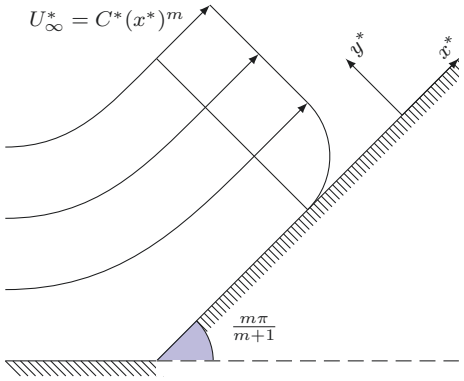

Figure 1: Schematic diagram of the boundary-layer flow over a wedge inclined at an angle $\theta = m\pi/(m+1)$.

free-stream velocity is assumed to be $U^*_\infty = C^*(x^*)^m$, where C^* is a positive constant. Having made this assumption the boundary-layer equations are solved, in a self-similar fashion, via the introduction of the following stream functions

$$\psi^*_p = [\nu^*_p U^*_\infty (x^*)^{1+s}]^{1/2} f_p(Y), \quad \psi^*_c = (\nu^*_c U^*_\infty x^*)^{1/2} f_c(Y),$$

where $s = (3m-1)(n-1)/(n+1)$, the dimensionless similarity variable is $Y = y^*/L^*_j$, and the subscript $j = p, c$, denotes the fluid model in question. The respective non-dimensionalising lengthscales are defined as such

$$L^*_p = \left[\frac{\nu^*_p (x^*)^{1+s}}{U^*_\infty}\right]^{1/2}, \quad L^*_c = \left(\frac{\nu^*_c x^*}{U^*_\infty}\right)^{1/2}.$$

Given that $u^* = \partial\psi^*_j/\partial y^*$ and $v^* = -\partial\psi^*_j/\partial x^*$ the boundary-layer equations reduce to

$$\bar{\mu}_p f'''_p = m[(f'_p)^2 - 1] - \frac{m+1+s}{2} f_p f''_p, \tag{2a}$$

$$\bar{\mu}_c f''''_c = m[(f'_c)^2 - 1] - \frac{m+1}{2} f_c f''_c, \tag{2b}$$

where

$$\bar{\mu}_p = n|f''_p|^{n-1}, \quad \bar{\mu}_c = [1 + n(\lambda f''_c)^2][1 + (\lambda f''_c)^2]^{(n-3)/2}. \tag{2.2c,d}$$

We note that it is only in the case when $m = 1/3$ that λ, the dimensionless equivalent of λ^*, is independent of both the streamwise coordinate and the inviscid free-stream velocity. In this case the constant λ takes the form

$$\lambda = \lambda^* C^* (C^*/\nu^*_c)^{1/2}.$$

Table 1: Base flow data for shear-thinning boundary-layer flows over a wedge inclined at an angle of $\pi/4$. The values of the constant λ_n, are determined such that $\bar{\mu}_p(0) = \bar{\mu}_c(0)$.

n	$\bar{\mu}_j(0)$	λ_n
0.8	0.8411	1.2479
0.7	0.7487	1.3032
0.6	0.6459	1.3688
0.5	0.5318	1.4473
0.4	0.4068	1.5422

Furthermore, we observe that for shear-thinning 'power-law type' boundary-layer flows the constant s, is identically zero only in the case when $m = 1/3$. With this in mind, and to ensure the consistency of our self-similar solutions, we restrict our attention to wedge flows inclined at an angle of $\pi/4$.

The ODEs stated in (2) are solved subject to the boundary conditions

$$f_j(Y = 0) = f_j'(Y = 0) = 0, \quad f_j'(Y \to \infty) \to 1. \tag{3}$$

A fourth order Runge-Kutta integrator twinned with a Newton-Raphson searching routine was employed to solve (2) subject to (3). The procedure iterates on the unknown $f_j''(0)$ until the boundary condition at infinity is satisfied to within some desired tolerance. In addition to this a secondary searching routine was employed to ensure that the value of λ, for each n, is such that the viscosity at maximum shear-rate (at the wall) is identical for both the power-law and Carreau fluid models, this matched value is denoted λ_n. For each n in the range of interest the power-law system of equations were solved to determine $\bar{\mu}_p(0)$, the searching routine then ensured that the value of λ is such that $\bar{\mu}_p(0) = \bar{\mu}_c(0)$. As noted by Bird *et al.* [9], typically, for shear-thinning flows of this nature, $O(10^{-1}) < \lambda < O(10^2)$. The results presented in table 1 therefore show that the matched λ_n values are well within the range of what would be expected to be observed experimentally. In their experimental study, Wu & Thompson [10] note that the boundary-layer equations accurately model flat plate shear-thinning flow even for moderate values of the Reynolds number in the range $O(10^1) - O(10^2)$, this gives us confidence that these self-similar solutions are appropriate in the context of our linear stability analysis.

In figure 2 the velocity $U_j = f_j'$, and viscosity functions are plotted against the boundary-layer coordinate $y = Y/\delta$, where δ is the familiar Falkner-Skan non-dimensional displacement thickness. Denier & Dabrowski [7] have shown that solutions determined from the power-law model decay to the far-field algebraically and that this decay is strongly dependent on the fluid index n. In the limit as $y \to \infty$ they show that

$$f_p' = 1 + Ay^{(n+1)/(n-1)} + \cdots, \tag{4}$$

where A is a constant of integration. In this case we find that fully converged

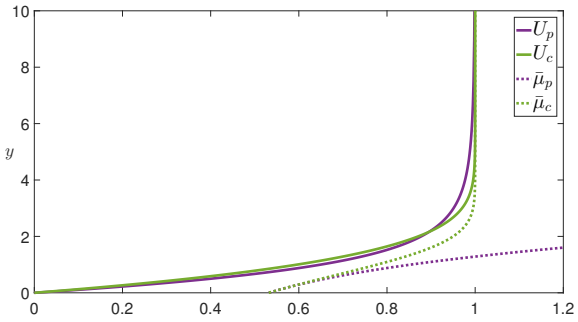

Figure 2: Velocity and viscosity profiles for the shear-thinning boundary-layer flow over a wedge inclined at an angle of $\pi/4$. The solid lines represent the velocity profiles whilst the dashed lines represent the viscosity profiles. In each case the fluid index is set to $n = 0.5$. The y-axis has been truncated at $y = 10$.

base flow solutions are only realisable when $n > 1/3$, as such, in this study, we restrict our attention to shear-thinning flows where $n \geq 0.4$. To ensure the correct algebraic decay of the solutions we enforce an additional asymptotic boundary condition at some suitably large value of y. Differentiating (4) gives the following far-field condition

$$f_p'' = \frac{n+1}{(n-1)} \frac{f_p' - 1}{y}, \quad \text{as} \quad y \to \infty.$$

It is the imposition of this condition that ensures that the power-law solutions decay to the far-field in the correct manner. To accommodate for the slow decay of the power-law solutions the thickness of the computational boundary-layer was increased, as the fluid index was decreased, until fully converged results had been achieved. Due to the failings of the power-law model in regions of low shear-rate we find that $\bar{\mu}_p$ remains unbounded within the confines of the boundary-layer region. This unphysical result is readily observed in figure 2. Following Griffiths *et al.* [11] we find that solutions determined from the Carreau fluid model exhibit the same exponential decay into the far-field as the corresponding Newtonian solutions. Due to the choice of non-dimensional parameters the Carreau viscosity function is essentially normalised such that $\bar{\mu}_c(y \to \infty) \to 1$.

In order to derive a governing set of linear disturbance equations the physical quantities specified in (1) are non-dimensionalised using the length, time, velocity and pressure scales δ^*, δ^*/U_∞^*, U_∞^* and $\rho^*(U_\infty^*)^2$, respectively. This choice of non-dimensional variables leads to the following definitions of the non-Newtonian Reynolds numbers

$$\mathcal{R}_p = \frac{\rho^*(U_\infty^*)^{2-n}(\delta^*)^n}{k^*} = \delta^{n-1}\frac{U_\infty^*\delta^*}{\nu_p^*}, \quad R_c = \frac{U_\infty^*\delta^*}{\nu_c^*},$$

where $\delta^* = \delta L_j^*$. In order to construct a comparative analysis between the two

non-Newtonian models we set

$$R_p = \delta^{1-n}\mathcal{R}_p = \frac{U_\infty^* \delta^*}{\nu_p^*}.$$

Utilising these definitions we arrive at following system of dimensionless equations

$$\frac{\partial u}{\partial x} + \frac{\partial v}{\partial y} = 0, \tag{5a}$$

$$\left(\frac{\partial}{\partial t} + u\frac{\partial}{\partial x} + v\frac{\partial}{\partial y}\right) u = -\frac{\partial p}{\partial x} + \frac{1}{R_j}\left\{2\frac{\partial}{\partial x}\left(\mu_j \frac{\partial u}{\partial x}\right) + \frac{\partial}{\partial y}\left[\mu_j\left(\frac{\partial u}{\partial y} + \frac{\partial v}{\partial x}\right)\right]\right\}, \tag{5b}$$

$$\left(\frac{\partial}{\partial t} + u\frac{\partial}{\partial x} + v\frac{\partial}{\partial y}\right) v = -\frac{\partial p}{\partial y} + \frac{1}{R_j}\left\{2\frac{\partial}{\partial y}\left(\mu_j \frac{\partial v}{\partial y}\right) + \frac{\partial}{\partial x}\left[\mu_j\left(\frac{\partial u}{\partial y} + \frac{\partial v}{\partial x}\right)\right]\right\}, \tag{5c}$$

where

$$\mu_p = |\dot{\gamma}|^{n-1}, \quad \mu_c = [1 + (\lambda\dot{\gamma})^2]^{(n-1)/2}, \tag{2.4d,e}$$

and

$$\dot{\gamma} = \left\{\left[\left(\frac{\partial u}{\partial y}\right) + \left(\frac{\partial v}{\partial x}\right)\right]^2 + 2\left[\left(\frac{\partial u}{\partial x}\right)^2 + \left(\frac{\partial v}{\partial y}\right)^2\right]\right\}^{1/2}. \tag{2.4f}$$

We now invoke the standard parallel flow approximation, in which the disturbance wavelength is assumed short compared to the development length-scale of the boundary layer, and so the basic flow can be taken to be independent of the streamwise coordinate x^*. Having done so we perturb u, v and p as such

$$\begin{aligned} u(x,y,t) &= U_j(y) + \varepsilon\tilde{u}(x,y,t), \\ v(x,y,t) &= \quad\quad + \varepsilon\tilde{v}(x,y,t), \\ p(x,y,t) &= p_0 \quad\quad + \varepsilon\tilde{p}(x,y,t), \end{aligned}$$

where here the amplitude of the disturbances is characterised by the small parameter $\varepsilon \ll 1$. Then, from (5), we arrive at a generalised Newtonian system of linear disturbance equations

$$\frac{\partial \tilde{u}}{\partial x} + \frac{\partial \tilde{v}}{\partial y} = 0, \tag{6a}$$

$$\left(\frac{\partial}{\partial t} + U_j\frac{\partial}{\partial x}\right)\tilde{u} + U_j'\tilde{v} = -\frac{\partial \tilde{p}}{\partial x} + \frac{1}{R_j}\left[\bar{\mu}_j\left(\frac{\partial^2\tilde{u}}{\partial x^2} + \frac{\partial^2\tilde{u}}{\partial y^2}\right) + \bar{\mu}_j'\left(\frac{\partial\tilde{u}}{\partial y} + \frac{\partial\tilde{v}}{\partial x}\right) - 2\bar{\bar{\mu}}_j\frac{\partial^2\tilde{u}}{\partial x^2}\right], \tag{6b}$$

$$\left(\frac{\partial}{\partial t} + U_j\frac{\partial}{\partial x}\right)\tilde{v} = -\frac{\partial \tilde{p}}{\partial y} + \frac{1}{R_j}\left[\bar{\mu}_j\left(\frac{\partial^2\tilde{v}}{\partial x^2} + \frac{\partial^2\tilde{v}}{\partial y^2}\right) + 2(\bar{\mu}_j - \bar{\bar{\mu}}_j)'\frac{\partial\tilde{v}}{\partial y} - 2\bar{\bar{\mu}}_j\frac{\partial^2\tilde{v}}{\partial y^2}\right], \tag{6c}$$

where here the primes denote differentiation with respect to y and the viscosity functions $\bar{\mu}_j$ and $\bar{\bar{\mu}}_j$ are defined as

$$\bar{\mu}_p = n|U_p'|^{n-1}, \qquad \bar{\mu}_c = [1 + n(\lambda U_c')^2][1 + (\lambda U_c')^2]^{(n-3)/2}, \tag{2.5d,e}$$

$$\bar{\bar{\mu}}_p = (n-1)|U_p'|^{n-1}, \quad \bar{\bar{\mu}}_c = (n-1)(\lambda U_c')^2[1 + (\lambda U_c')^2]^{(n-3)/2}. \tag{2.5f,g}$$

Further to this, if the perturbation quantities are assumed to have the normal mode form

$$[\tilde{u}(x,y,t), \tilde{v}(x,y,t), \tilde{p}(x,y,t)] = [\hat{u}(y), \hat{v}(y), \hat{p}(y)]e^{\mathrm{i}(\alpha x - \omega t)},$$

where $\alpha = \alpha_\mathrm{r} + \mathrm{i}\alpha_\mathrm{i}$, is the streamwise wavenumber and ω is the perturbation frequency, then (6) can be reduced to a set of ODEs that govern the linear stability characteristics of the flow

$$\mathrm{i}\alpha\hat{u} + \hat{v}' = 0, \tag{7a}$$

$$R_j[\mathrm{i}(\alpha U_j - \omega)\hat{u} + U_j'\hat{v} + \mathrm{i}\alpha\hat{p}] = \bar{\mu}_j(\hat{u}'' - \alpha^2\hat{u}) + \bar{\mu}_j'(\hat{u}' + \mathrm{i}\alpha\hat{v}) + 2\alpha^2\bar{\bar{\mu}}_j\hat{u}, \tag{7b}$$

$$R_j[\mathrm{i}(\alpha U_j - \omega)\hat{v} + \hat{p}'] = \bar{\mu}_j(\hat{v}'' - \alpha^2\hat{v}) + 2[\bar{\mu}_j'\hat{v}' - (\bar{\bar{\mu}}_j\hat{v}')']. \tag{7c}$$

It should be noted that these ODEs are inclusive of the viscosity perturbation terms that owe from a Taylor expansion of the viscosity functions defined in (2). The familiar Newtonian system of equations is returned when $n = 1$.

System (7) represents a coupled quadratic eigenvalue problem for α of the form

$$(A_2\alpha^2 + A_1\alpha + A_0)\hat{Q} = 0,$$

where A_0, A_1, and A_2 are matrices with entries determined by the factors multiplying the zeroth, first and second-order α terms, respectively. The vector of eigenfunctions is $\hat{Q} = (\hat{u}, \hat{v}, \hat{p})^\mathrm{T}$. This coupled quadratic eigenvalue problem is solved subject to the boundary conditions

$$\hat{u}(y=0) = \hat{v}(y=0) = \hat{v}'(y=0) = 0, \tag{8a}$$

$$\hat{u}(y\to\infty) \to \hat{v}(y\to\infty) \to \hat{p}(y\to\infty) \to 0. \tag{8b}$$

To ensure the no-slip criterion is satisfied the velocity perturbations at the wall must equal zero. Additionally, the continuity equation dictates that the first derivation of $\hat{v}$ must also be zero here. We seek decaying perturbations thus $\hat{u}$, $\hat{v}$ and $\hat{p}$ must tend to zero as $y \to \infty$.

The neutral temporal and spatial stability of the system was determined using a Chebyshev polynomial discretisation method. The Gauss-Lobatto collocation points were transformed into the physical domain via an exponential map. The boundary conditions (8) were then imposed at $y = 0$ and $y = y_\mathrm{max}$, where the value of y_max is such that the steady mean flow results had converged to within some desired tolerance, typically, 10^{-10}. In each case considered it was found that the value of y_max that ensured mean flow convergence also ensured that the both the real and imaginary parts of the solution for α had converged

to at least four decimal places. When considering the Carreau model flows, that exhibit exponential decay to the far-field, a sufficiently large value of y was found to be $y_{\max} = 20$. In these cases 100 collocation points were distributed, via the exponential map, between the upper and lower boundaries. Further increasing the number of collocation points revealed no discernible difference in the numerical results. In the power-law cases, where the far-field mean flow decay is algebraic, the number of collocation points was increased proportionally with the necessary increase in the value of $y_{\max}$. The stability equations (7) were then solved in terms of primitive variables at each of the collocation points, excluding those on the boundary edges. This global eigenvalue solution method is favourable when compared to local (Orr-Sommerfeld) approaches as it is possible to simultaneously obtain all of the eigenvalues and eigenvectors.

This numerical routine was verified against the familiar neutral stability results of the Newtonian Blasius boundary-layer problem ($m = 0$). It was found that $R^{\text{crit}} = 519.1$, $\alpha^{\text{crit}} = 0.304$, and $\omega^{\text{crit}} = 0.1208$, which is excellent agreement with the results of Schmid & Henningson [12], for example.

It proves pertinent, at this stage, to introduce the quantities that will be useful for interpreting the linear stability characteristics of the flows. The non-dimensional frequencies that are independent of the streamwise coordinate x^*, are defined as such

$$(F_p, F_c) = \frac{\omega}{(R_p, R_c)} = \frac{\omega^*(\nu_p^*, \nu_c^*)}{(U_\infty^*)^2}.$$

In addition to this, the measure of the linear growth of a disturbance as it propagates downstream is given by

$$N_j = \ln\left(\frac{A}{A_0}\right) = -\frac{2}{\delta^2}\int_{R_j^0}^{R_j} \alpha_{\text{i}}\, \mathrm{d}R_j,$$

where the maximum value of N_j is the so-called N exponent utilised in the familiar e^N calculations. Here A is the amplitude of the perturbation. For a given disturbance with frequency F_j, the value of R_j^0, is the point at which the flow first exhibits linear instability. The corresponding value of A_0 is the amplitude of the disturbance at this location.

3 Neutral Stability Results

In the first instance we solve (7) subject to (8) and determine the curves of neutral stability. Given that ω is strictly real, these are the points where, for a given value of R_j, $\alpha_{\text{i}} = 0$. Neutrally stable results are presented in figure 3 in both the (R_j, α) and (R_j, F_j) planes. For both non-Newtonian models we observe that as the shear-thinning effect becomes more pronounced (n decreases), the critical Reynolds number of the flow increases and the area encompassed by the neutral stability curve decreases. These results suggest that shear-thinning has the effect of stabilising the boundary-layer flow. Although these results are qualitatively similar, it should be noted that there is a marked difference between the

Table 2: Comparison of the critical values of the Reynolds number and the corresponding critical value of F_j. For each n the base flow data has been matched such that the viscosity at the wall is identical for both the power-law and Carreau fluid models.

n	R_p^{crit}	$F_p^{\text{crit}} \times 10^6$	R_c^{crit}	$F_c^{\text{crit}} \times 10^6$
0.8	10191.4	3.523	8307.4	4.358
0.7	11768.1	2.923	8814.0	3.858
0.6	13486.0	2.447	9507.3	3.313
0.5	15201.5	2.138	10502.4	2.704
0.4	16606.7	1.963	12053.9	2.066

critical values associated with the power-law and Carreau fluid models. This critical data is presented in table 2.

When considering the modified Carreau model, shear-thinning effects can be further amplified by increasing the value of the material time constant, λ. The results presented thus far have considered only the case when $\lambda = \lambda_n$. However, as noted by Bird *et al.* [9], the range of experimentally observed λ values can vary by at least two orders of magnitude for shear-thinning polymer solutions.

In their shear-thinning Poiseuille flow study Nouar *et al.* [1] argue that, for confined shear flows, the Reynolds number should be redefined in terms of what they describe as *the tangent viscosity at the wall*. The authors note that this is a reasonable assumption to make as the T-S waves originate in a viscous layer close to the wall. The same argument holds in this case and it is important to consider this scaling when presenting results when $\lambda \neq \lambda_n$. Thus far, when comparing solutions between the two non-Newtonian models the decision to match the base flow results such that $\bar{\mu}_p(0) = \bar{\mu}_c(0)$, has essentially negated the need to scale the Reynolds numbers. However, when $\lambda \neq \lambda_n$ the value of $\bar{\mu}_p(0)$ will not match that of $\bar{\mu}_c(0)$ and in these cases it is appropriate to scale R_c as such

$$\tilde{R}_c = \frac{\bar{\mu}_p(0)}{\sigma} R_c,$$

where, for a given value of λ, σ is the value of $\bar{\mu}_c$ at the wall. When $\lambda = \lambda_n$, $\sigma = \bar{\mu}_c(0) = \bar{\mu}_p(0)$, and $\tilde{R}_c = R_c$. It is important to note that our definition of the viscosity function is directly equivalent to Nouar *et al.*'s 'tangent' viscosity.

Using a bisection algorithm we find, for a fixed value of λ, the corresponding critical values the unscaled and scaled Reynolds numbers. The results presented in figure 4 demonstrate the importance of appropriately scaling the Reynolds number. In both cases, for each n in the range of interest, we find that there exists a λ value that maximises the stabilising effect of shear-thinning (with respect to the onset of linear instability), and this value is henceforth denoted $\lambda_{\max}$. If the viscosity at maximum shear-rate is not accounted for in the definition of the Reynolds number then we find that for suitably large values of λ, shear-thinning has the effect of destabilising the boundary-layer flow, when compared to Newtonian benchmark. However, this behaviour is not observed

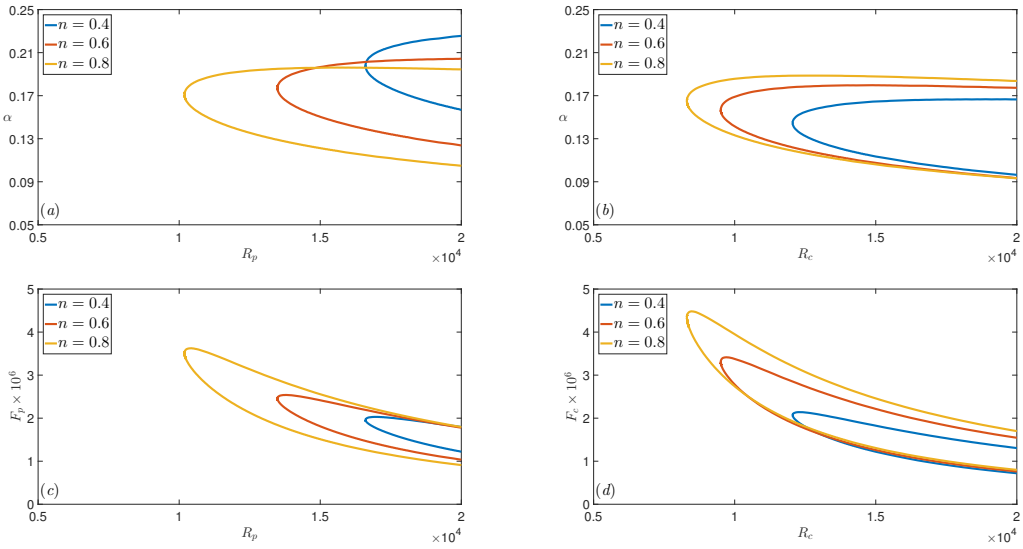

Figure 3: Temporal and spatial neutral stability curves for a range of shear-thinning fluids. Results owing from the power-law and Carreau fluid models are presented in (a) & (c) , and (b) & (d) , respectively. In (a) & (b) , and (c) & (d) the streamwise wavenumber and the frequency parameter is plotted against the non-Newtonian Reynolds number, respectively.

if the Reynolds number is appropriately scaled. Indeed, in this case, for each n, we find that as $\lambda \to \infty$ the critical value of the Reynolds number tends to a well defined asymptotic limit.

In order to quantify the growth of the disturbances we plot the variation of $\ln(A/A_0)$ against the Reynolds number for a range of dimensionless frequency values. As is typical for two-dimensional boundary-layer flows we find that higher frequency disturbances are amplified at lower Reynolds numbers whereas lower frequencies become unstable at larger values of the Reynolds number. For each constant value of F_j, the N_j-factor curve is tangent to the curve representing the variation of $\ln(A/A_0)$. The results presented in figure 5 demonstrate that for the same fixed value of the fluid index the gradient of the N_c-factor curve is noticeably steeper than the equivalent result determined from the power-law model. In a very broad sense[2], this would suggest that the power-law model under predicts the relative growth of the linearly unstable disturbances when compared to the Carreau fluid model. This result is in keeping with the findings presented in figure 3 where we see that when $\lambda = \lambda_n$, for a fixed value of the fluid index, the power-law model first exhibits linear instability at a much larger value of the Reynolds number.

[2]The relative merits and shortcomings of the e^N method in predicting transition in two-dimensional boundary-layer flows are addressed in the review article by van Ingen [13].

Table 3: Critical $\tilde{R}_c$ and $\tilde{F}_c = \omega/\tilde{R}_c$, values for shear-thinning flows modelled using the modified Carreau relationship. The value of the material time constant has been determined in order to maximise the critical value of the scaled Reynolds number.

n	$\lambda_{\max}$	$\tilde{R}_c^{\text{crit}}$	$\tilde{F}_c^{\text{crit}} \times 10^6$
0.8	5.4445	10377.0	3.373
0.7	4.7112	12258.5	2.659
0.6	4.2199	14601.4	2.068
0.5	3.4285	17487.5	1.573
0.4	3.0217	21498.9	1.130

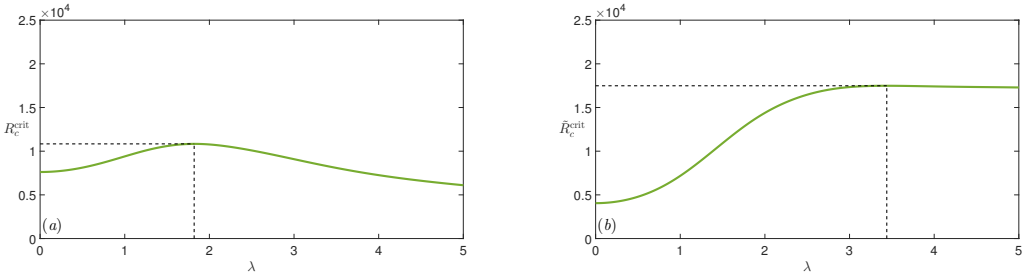

Figure 4: Variation of the unscaled and scaled critical Reynolds numbers with respect to the material time constant. In this case the fluid index takes the value $n = 0.5$. The dashed lines indicate the location of the optimum λ values.

As a point of reference the Newtonian N-factor curve has been included in both plots contained within figure 5. Working under the assumption that the onset of transition occurs when the N-factor reaches a predetermined value (for the purposes of this discussion, in keeping with van Ingen [13], we set this value at $N = 9$), we observe that both fluid models predict that shear-thinning delays the transition to turbulence. Indeed, for both models, for each n in the range of interest, we find that the N-factor curves are shifted along the R-axis suggesting that shear-thinning will always have the effect of delaying transition, even when n is only very marginally less than unity.

It should be noted here that the N-factor value of 9 is based on an empiricism and therefore does not necessarily predict the exact location of transition.

4 Energy Analysis

In order to physically quantify the stability results presented in §3, we perform an energy balance calculation akin to that of Cooper & Carpenter [14], who considered the flow due to a compliant rotating disk. The calculation presented here indicates the relative influences of the energy transfer mechanisms that are

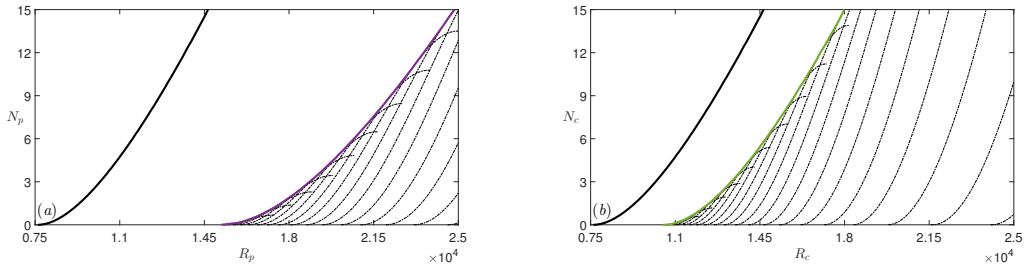

Figure 5: N-factor curves for shear-thinning fluids with fluid index $n = 0.5$. The integrated growth rates for a range of dimensionless frequency values are given by the dashed lines. The N_j-factor curve is tangent to the maximum value of these total amplification curves. The Carreau fluid results were obtained by setting $\lambda = \lambda_n$. In both cases the Newtonian solution (solid black curve) has been included as a comparative aid.

associated with two-dimensional boundary-layer flows of this nature.

Energy production and dissipation terms are determined from the equation for kinetic energy. As is commonplace in the literature we define the kinetic energy of a two-dimensional disturbance as such

$$\tilde{e} = \frac{\tilde{u}^2 + \tilde{v}^2}{2}.$$

Multiplying (6b), and (6c), by $\tilde{u}$, and $\tilde{v}$, respectively, and summing the resulting equations, we arrive at a generalised Newtonian kinetic energy equation

$$\begin{aligned}\left(\frac{\partial}{\partial t} + U_j\frac{\partial}{\partial x}\right)\tilde{e} + U_j'\tilde{u}\tilde{v} = &-\frac{\partial(\tilde{u}\tilde{p})}{\partial x} - \frac{\partial(\tilde{v}\tilde{p})}{\partial y} + \frac{\bar{\mu}_j}{R_j}\left[\frac{\partial(\tilde{v}\tilde{q})}{\partial x} - \frac{\partial(\tilde{u}\tilde{q})}{\partial y} - \tilde{q}^2\right] \\ &- \frac{\bar{\bar{\mu}}_j}{R_j}\left[\frac{\partial(\tilde{v}\tilde{r})}{\partial x} - \frac{\partial(\tilde{u}\tilde{r})}{\partial y} - \tilde{r}^2\right] \\ &+ \frac{\bar{\mu}_j'}{R_j}\left[\frac{\partial(\tilde{u}\tilde{v})}{\partial x} + \frac{\partial\tilde{e}}{\partial y}\right] + \frac{(\bar{\mu}_j - \bar{\bar{\mu}}_j)'}{R_j}\frac{\partial\tilde{v}^2}{\partial y},\end{aligned}$$

where

$$\tilde{q} = \frac{\partial\tilde{v}}{\partial x} - \frac{\partial\tilde{u}}{\partial y}, \quad \text{and} \quad \tilde{r} = \frac{\partial\tilde{u}}{\partial x} - \frac{\partial\tilde{v}}{\partial y}.$$

Averaging the perturbations over a single time period and integrating across

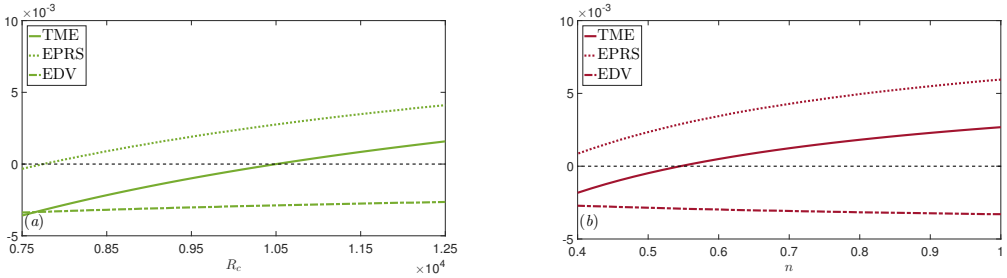

Figure 6: Variation of the total mechanical energy, energy production due to Reynolds stresses, and energy dissipation due to viscosity with R_c, and n, respectively. Points where the solid curve cross the dashed black line indicate a shift from linearly stable to linearly unstable flow. In (a) the shear-thinning index is set to $n = 0.5$, whilst in (b) the Reynolds number is fixed such that $R_c = 1 \times 10^4$.

the thickness of the boundary-layer gives the following integral energy equation

$$\begin{aligned}\frac{\mathrm{d}E}{\mathrm{d}x} =& -\int_0^\infty U_j' < \tilde{u}\tilde{v} > \mathrm{d}y - \frac{1}{R_j}\int_0^\infty \bar{\mu}_j < \tilde{q}^2 > \mathrm{d}y - \frac{\mathrm{d}}{\mathrm{d}x}\int_0^\infty < \tilde{u}\tilde{p} > \mathrm{d}y \\ &+ \frac{1}{R_j}\Bigg\{\frac{\mathrm{d}}{\mathrm{d}x}\int_0^\infty \bar{\mu}_j < \tilde{v}\tilde{q} > -\bar{\bar{\mu}}_j < \tilde{v}\tilde{r} > +\bar{\mu}_j' < \tilde{u}\tilde{v} > \mathrm{d}y \\ &\quad + \int_0^\infty \bar{\mu}_j' < \tilde{u}\tilde{q} > -\bar{\bar{\mu}}_j' < \tilde{u}\tilde{r} > +\bar{\bar{\mu}}_j < \tilde{r}^2 > -\bar{\mu}_j'' < \tilde{e} > -(\bar{\mu}_j - \bar{\bar{\mu}}_j)'' < \tilde{v}^2 > \mathrm{d}y\Bigg\},\end{aligned} \tag{9}$$

where $E = \int_0^\infty U_j < \tilde{e} > \mathrm{d}y$, is the total kinetic energy which is being convected past a given location.

In his Newtonian study Morris [15] has shown that the first term within the braces is negligible. Our calculations reveal that this term remains negligible in spite of the appearance of a non-constant viscosity function. The remaining seven terms within the braces appear because of the non-Newtonian constitutive viscosity relationship, and vanish in the Newtonian limit. Somewhat surprisingly we find that all of these terms are also negligible. This suggests that the source of any non-Newtonian stabilising/destabilising effects owe largely from the modification of the base flow profiles, not the additional viscous terms that appear in the governing perturbation equations.

Given that the perturbations have the normal mode form, normalising (9) with respect to $\int_0^\infty U_j < \hat{e} > + < \hat{u}\hat{p} > \mathrm{d}y$, gives

$$\underbrace{-2\alpha_\mathrm{i}}_{\text{TME}} \simeq \underbrace{\int_0^\infty U_j' < \hat{u}\hat{v} > \mathrm{d}y}_{\text{EPRS}} + \underbrace{\frac{1}{R_j}\int_0^\infty \bar{\mu}_j < \hat{q}^2 > \mathrm{d}y}_{\text{EDV}}, \tag{10}$$

where $\hat{e} = (1/2)(\hat{u}^2 + \hat{v}^2)$, $\hat{q} = \mathrm{i}\alpha\hat{v} - \hat{u}'$, and $< \hat{x}\hat{y} >= \hat{x}\hat{y}^\star + \hat{x}^\star\hat{y}$ (* indicates

complex conjugate). The term on the left of (10) is understood to be the Total Mechanical Energy (TME) of a given disturbance. The first term on the right–hand side is the Energy Production due to Reynolds Stresses (EPRS), whilst the second corresponds to the Energy Dissipation due to Viscosity (EDV).

When energy production outweighs energy dissipation the eigenmode in question is amplified. This indicates instability and is consistent with the condition that if $\alpha_{\mathrm{i}} < 0$, the flow is linearly unstable.

In figure 6 we present energy balance calculations for the most unstable eigenmode ($\alpha_{\mathrm{i}} = \max(\alpha_{\mathrm{i}})$) for ($a$) a range of Reynolds numbers at a fixed value of $n = 0.5$, and (b) for a range of shear-thinning values given that $R_c = 1 \times 10^4$. In each case considered the sum of the energy production (EPRS) and dissipation terms (EDV) is equal to $-2\alpha_{\mathrm{i}}$, to an order of at least five decimal places. This precision indicates the relatively minuscule influence of the aforementioned omitted terms. From both figures it is clear that the energy production due to Reynolds stresses remains the dominating physical mechanism for the onset of instability. Most interestingly we see that the energy dissipation due to viscosity is essentially invariant with the fluid index. This result supports our earlier conjecture that the form of the streamwise velocity profile plays the largest role in determining the stability characteristics of generalised Newtonian flows, and, in fact, that the variation of viscosity across the boundary layer has very little influence on linear stability results. In the interest of brevity we choose not to present power-law solutions here but note that qualitatively similar results are obtained. The findings suggest that shear-thinning has the effect of reducing the energy production due to Reynolds stresses, resulting in a reduction of the total mechanical energy available to destabilise the T-S waves.

5 Discussion & Conclusions

The linear stability of the shear-thinning boundary-layer flow over an inclined flat plate has been considered for two of the more popular generalised Newtonian viscosity models. This work was motivated by previous studies that indicate that the effect of shear-thinning can act to stabilise confined shear flows. The results presented within this report suggest that the addition of shear-thinning agents could act as a passive control mechanism for unconfined boundary-layer flows.

Terms arising from the perturbation of the respective viscosity functions were included in the derivation of the linear disturbance equations. The subsequent equations were solved using a Chebyshev collocation scheme. Results from the power-law formulation of the problem suggest that the effect of shear-thinning will act to significantly stabilise the boundary-layer flow. This result is qualitatively supported by solutions obtained under the Carreau fluid model. When considering the Carreau model we find that there exists an optimum value of the material time constant that maximises this stabilising effect. These results are presented above in table 3. In agreement with Nouar *et al.* [1], we note the importance of appropriately scaling the Reynolds number as it is possible

to arrive at differing conclusions depending on the choice of viscosity scale. In the scaled frame of reference we find that this stabilising effect is maintained for large values of λ. However, this is not the case if the viscosity at the wall is ignored in the definition of the Reynolds number. Unsurprisingly, the optimum value of λ depends on the fluid index; we find that the value of $\lambda_{\max}$ decreases linearly with n. Additional calculations have shown that, irrespective of the choice of viscosity scale, the Carreau fluid model will, for at least specific range of λ values, always exhibit stabilising behaviour.

The linear growth of the downstream disturbances were interpreted in the context of the total amplification of the streamwise wavenumbers. The growth of the linear disturbances is observed to be greater under the Carreau fluid model when compared to the corresponding results obtain from the power-law regime. Nevertheless, for all the shear-thinning cases considered within this investigation, the linear growth, and associated N-factor results, indicate stabilisation when compared to the Newtonian benchmark. This suggest that the onset of transition will be delayed for two-dimensional boundary-layer flows in the presence of shear-thinning.

Results from the generalised Newtonian integral energy equation reveal that, irrespective of the introduction of shear-thinning, the dominate energy transfer mechanism within the system remains the energy production due to Reynolds stresses. Shear-thinning has essentially no effect on the energy dissipation. This result implies that the relative dissipation is sensitive to the precise form of the streamwise steady flow profile, not the variation of viscosity across the boundary-layer.

The arguments regarding the applicability of parallel linear stability theory (LST) to growing two-dimensional boundary-layer flows is clearly relevant to this investigation. The framework presented here is unable to capture either the slow spatial growth of the boundary layer flow or the nonlinear development of the disturbances. As demonstrated in this study the critical Reynolds number for favourable pressure gradient flows is moderately large and so non-parallel effects, which become more important at lower Reynolds, are likely to be less important when compared to studies that consider zero or adverse pressure gradient flows. The importance of nonlinear effects on the transition to turbulence is well documented within the literature and this is something that is currently outside of the scope of this investigation. Newtonian nonlinear and non-parallel investigations reveal that, in general, LST gives an overestimate for the location of the onset of instability, see, for example, Herbert [16]. Similarly, although still widely used in industry for the prediction of transition, the e^N method suffers from the inability to incorporate nonlinear mechanisms and the initial amplitude of the disturbances. Taking these factors into account this study represents the first step in determining the potentially advantageous effect that shear-thinning can have on the instability and transition of unconfined two-dimensional boundary-layer flows.

A natural extension of this investigation would be to consider a high Reynolds number asymptotic description of both the upper and lower branch neutral modes. In this case a self-consistent description of the flow would be obtain-

able. An analytical study such as this would reveal the important factors that contribute to any stabilising/destabilising effects at large Reynolds numbers. One would hope that the results from this type of investigation would support the hypothesis that the stability of the flow is governed largely by the form of the streamwise base flow profiles and not the variation of viscosity across the boundary layer.

References

[1] Nouar C, Bottaro A, Brancher JP. 2007 Delaying transition to turbulence in channel flow: revisiting the stability of shear-thinning fluids. *J. Fluid Mech.* **592**, 177–194.

[2] Nouar C, Frigaard I. 2009 Stability of plane Couette-Poiseuille flow of shear-thinning fluid *Phys. Fluids.* **21**, 064104.

[3] Alibenyahia B, Lemaitre C, Nouar C, Ait-Messaoudene N. 2012 Revisiting the stbility of circular Couette flow of shear-thinning fluids *J. Non-Newtonian Fluid Mech.* **183-184**, 37-51.

[4] Griffiths PT, Stephen SO, Bassom AP, Garrett SJ. 2014 Stability of the boundary-layer on a rotating disk for power-law fluids *J. Non-Newtonian Fluid Mech.* **207**, 1-6.

[5] Griffiths PT, Stephen SO, Garrett SJ. 2014 The neutral curve for stationary disturbances in rotating disk flow for power-law fluids *J. Non-Newtonian Fluid Mech.* **213**, 83-81.

[6] Acrivos A, Shah MJ, Petersen EE. 1960 Momentum and Heat Transfer in Laminar Boundary-Layer Flows of Non-Newtonian Fluids Past External Surfaces *AIChE J.* **6**, 312-317.

[7] Denier JP, Dabrowski PP. 2004 On the boundary layer equations for power-law fluids *Proc. R. Soc. Lond.* A **460**, 3143-3158.

[8] Dabrowski PP. 2009 Boundary-layer Flows in non-Newtonian Fluids *Ph.D. thesis, School of Mathematical Sciences, The University of Adelaide.*

[9] Bird RB, Armstrong RC, Hassager O. 1987 *Dynamics of Polymeric Liquids* Wiley 2nd edn.

[10] Wu J, Thompson MC. 1996 Non-Newtonian shear-thinning flows past a flat plate *J. Non-Newtonian Fluid Mech.* **66**, 127-144.

[11] Griffiths PT, Gallagher MT, Stephen SO. 2016 The effect of non-Newtonian viscosity on the stability of the Blasius boundary layer *Phys. Fluids* **28**, 074107.

[12] Schmid PJ, Henningson DS. 2001 *Stability and Transition in Shear Flows* Springer

[13] van Ingen JL. 2008 The e^N method for transition prediction. Historical review of work at TU Delft *AIAA Paper 2008-3830.*

[14] Cooper AJ, Carpenter PW. 1997 The stability of rotating-disc boundary-layer flow over a compliant wall. Part 1. Type I and II instabilities *J. Fluid Mech.* **350**, 231-259.

[15] Morris PJ. 1976 The spatial viscous instability of antisymmetric jets *J. Fluid Mech.* **77**, 511-529.

[16] Herbert T. 1997 Parabolized stability equations *Annu. Rev. Fluid. Mech.* **29**, 245-283.